echnical Memorandum NESS 66

A SUMMARY OF THE RADIOMETRIC TECHNOLOGY MODEL OF THE OCEAN SURFACE IN THE MICROWAVE REGION

John C. Alishouse

Washington, D.C.
March 1975

noaa NATIONAL OCEANIC AND ATMOSPHERIC ADMINISTRATION / National Environmental Satellite Service

National Environmental Satellite Service Series

The National Environmental Satellite Service (NESS) is responsible for the establishment and operation of the environmental satellite systems of NOAA.

NOAA Technical Memorandums facilitate rapid distribution of material that may be preliminary in nature and so may be published formally elsewhere at a later date. Publications 1 through 20 and 22 through 25 are in the earlier ESSA National Environmental Satellite Center Technical Memorandum (NESCTM) series (listed in NESS 30). The current NOAA Technical Memorandum NESS series includes 21, 26, and subsequent issuances.

Publications listed below are available from the National Technical Information Service, U.S. Department of Commerce, Sills Bldg., 5285 Port Royal Road, Springfield, Va. 22151. Prices on request. Order by accession number (given in parentheses). Information on memorandums not listed below can be obtained from Environmental Data Service (D831), 3300 Whitehaven St., NW, Washington, D.C. 20235.

NOAA Technical Memorandums

NESS 27 A Review of Passive Microwave Remote Sensing. James J. Whalen, March 1971, 8 pp. (COM-72-10546)

NESS 28 Calculation of Clear-Column Radiances Using Airborne Infrared Temperature Profile Radiometer Measurements Over Partly Cloudy Areas. William L. Smith, March 1971, 12 pp. (COM-71-00556)

NESS 29 The Operational Processing of Solar Proton Monitor and Flat Plate Radiometer Data. Henry L. Phillips and Louis Rubin, May 1972, 20 pp. (COM-72-10719)

NESS 30 Limits on the Accuracy of Infrared Radiation Measurements of Sea-Surface Temperature From a Satellite. Charles Braun, December 1971, 28 pp. (COM-72-10898)

NESS 31 Publications and Final Reports on Contracts and Grants, 1970. NESS, December 1971, 6 pp. (COM-72-10303)

NESS 32 On Reference Levels for Determining Height Profiles From Satellite-Measured Temperature Profiles. Christopher M. Hayden, December 1971, 15 pp. (COM-72-50393)

NESS 33 Use of Satellite Data in East Coast Snowstorm Forecasting. Frances C. Parmenter, February 1972, 21 pp. (COM-72-10482)

NESS 34 Chromium Dioxide Recording--Its Characteristics and Potential for Telemetry. Florence Nesh, March 1972, 10 pp. (COM-72-10644)

NESS 35 Modified Version of the Improved TIROS Operational Satellite (ITOS D-G). A. Schwalb, April 1972, 48 pp. (COM-72-10547)

NESS 36 A Technique for the Analysis and Forecasting of Tropical Cyclone Intensities From Satellite Pictures. Vernon F. Dvorak, June 1972, 15 pp. (COM-72-10840)

NESS 37 Some Preliminary Results of 1971 Aircraft Microwave Measurements of Ice in the Beaufort Sea. Richard J. DeRycke and Alan E. Strong, June 1972, 8 pp. (COM-72-10847)

NESS 38 Publications and Final Reports on Contracts and Grants, 1971. NESS, June 1972, 7 pp. (COM-72-11115)

NESS 39 Operational Procedures for Estimating Wind Vectors From Geostationary Satellite Data. Michael T. Young, Russell C. Doolittle, and Lee M. Mace, July 1972, 19 pp. (COM-72-10910)

NESS 40 Convective Clouds as Tracers of Air Motion. Lester F. Hubert and Andrew Timchalk, August 1972, 12 pp. (COM-72-11421)

NESS 41 Effect of Orbital Inclination and Spin Axis Attitude on Wind Estimates From Photographs by Geosynchronous Satellites. Linwood F. Whitney, Jr., September 1972, 32 pp. (COM-72-11499)

NESS 42 Evaluation of a Technique for the Analysis and Forecasting of Tropical Cyclone Intensities From Satellite Pictures. Carl O. Erickson, September 1972, 28 pp. (COM-72-11472)

(Continued on inside back cover)

NOAA Technical Memorandum NESS 66

A SUMMARY OF THE RADIOMETRIC TECHNOLOGY MODEL OF THE OCEAN SURFACE IN THE MICROWAVE REGION

John C. Alishouse

Washington, D.C.
March 1975

UNITED STATES
DEPARTMENT OF COMMERCE
Frederick B. Dent, Secretary

NATIONAL OCEANIC AND
ATMOSPHERIC ADMINISTRATION
Robert M. White, Administrator

National Environmental
Satellite Service
David S. Johnson, Director

CONTENTS

TABLES

FIGURES

A SUMMARY OF THE RADIOMETRIC TECHNOLOGY MODEL OF THE OCEAN SURFACE IN THE MICROWAVE REGION

John C. Alishouse
National Environmental Satellite Service, NOAA, Washington, D.C.

ABSTRACT. Between November 1970 and March 1974, under a series of three contracts with the National Oceanic and Atmospheric Administration's National Environmental Satellite Service, Radiometric Technology, Inc., carried on studies to assess the potential of determining sea-surface temperature and roughness from a satellite-borne microwave radiometer. The final reports, consisting of 5 volumes containing a total of more than 1100 pages, represent a significant contribution to this particular area of research.

The model developed by Porter and Wentz is a two dimensional two-scale model in that it incorporates upwind and crosswind wave spectra and considers waves that are both large and small in comparison with the radiometer's wavelength. This technical memorandum presents the more significant results of Porter and Wentz in a less formidable matrix.

I. INTRODUCTION

Between November 1970 and March 1974, under a series of three contracts from the National Oceanic and Atmospheric Administration (NOAA), Radiometric Technology, Inc.,[1] carried on studies to assess the potential of determining sea-surface temperature and roughness from satellites utilizing a microwave radiometer. The final reports (Porter and Wentz[2] 1971, Porter and Wentz 1972, and Wentz 1974) consist of 5 volumes, contain more than 1,100 pages, and fill 4 in. on a bookshelf. They cover the development of a sophisticated model of the sea surface, which includes both capillary and gravity waves. The scope of the investigation, while completely analytical, nevertheless was quite extensive and investigated such factors as salinity, foam, wave spectra, polarization, and atmospheric attenuation to determine optimum frequencies and accuracy limitations. In view of the length and depth of the reports, as well as the evolutionary character of the results, a summary of the more important and final results was deemed appropriate.

Each contract final report contains a section of author-identified significant results or conclusions that were used as a basis for this summary. Relevant material contained elsewhere in the contract report then is presented to support the conclusions.

---

[1]Located at 28C Vernon Street, Wakefield, Massachusetts 01880

[2]Present address: F. J. Wentz and Associates, Box 162, Massachusetts Institute of Technology (MIT) Branch Post Office, Cambridge, Massachusetts 02139

One should note that not all conclusions and significant results identified by the authors of the contract reports are presented in this summary; there are two reasons for this. The first is that some of the results are modified to some extent by the inclusion of refinements in the model for sea-surface emissivity. It would be unfair both to the authors of the original work and to the readers of this summary if apparently contradictory or conflicting results were presented. Accordingly, only the last result is presented in such a case. In a few instances, the author of this summary has decided somewhat arbitrarily that some of the results were not sufficiently significant and so omitted them.

In addition, a one- to two-page summary of objectives, ranges of parameters, and other background material are presented to provide the reader with at least some background and context for the conclusions presented.

Finally, there has been some editorializing in the material in that reference citations have been changed to conform to NOAA format and a few figure legends have been changed so that the same symbols have the same meaning everywhere in this summary.

II. DISCUSSION OF "MICROWAVE RADIOMETRIC STUDY OF OCEAN SURFACE CHARACTERISTICS" (PORTER AND WENTZ 1971)

A. Summary

" The objective of this study was to investigate in considerable detail the microwave characteristics of calm, rough, and foam-covered ocean surfaces and to develop a technique for deriving thermodynamic ocean surface temperatures from brightness temperatures measured by an earth-orbiting radiometer. This investigation encompassed frequencies in the range 1 to 10 GHz (wavelength range of 30 to 3 cm) and was based on the use of a 1-dimensional geometric optics roughness model (Lynch and Wagner 1970) including shadowing and multiple scattering of radiant electro-magnetic energy. Provision is made in the model for characterizing surface roughness through the rms slope-versus-wind velocity relations previously established by other researchers (Cox and Munk 1954). Suitable foam and atmospheric models were superimposed on the roughness model.

"A wide variety of operating and environmental parameters were brought into the study, including both horizontal and vertical polarizations, an antenna beam nadir angle range of 0 to 60 degrees, wind velocities from 4 to 20 meters/sec., surface temperatures from 276 to 296 degrees Kelvin, salinities of 24 to 37 parts per thousand ($^{\circ}/_{oo}$), and atmospheric conditions ranging from clear sky to heavy rain. Following preliminary studies concerned with the dielectric properties of model sea water, specular emissivities, and specular brightness temperatures, an initial frequency optimization analysis was performed, this involving a total of twelve frequencies in the above range. Based on the response of brightness temperature to changes in surface temperature and the uncertainties introduced by the atmosphere at higher frequencies, the frequency span was compressed to the range 1.4 to 5 GHz. Concurrently, the salinity range was reduced to 31 to 37$^{\circ}/_{oo}$, thus eliminating river estuaries from further consideration.

"Rough ocean brightness temperatures were generated and a physical foam model was established. This presented some unusual problems because of the limited amount of information available on the physical structure of a given patch of foam and the percentage coverage of ocean surfaces by foam as a function of wind velocity. A decision was ultimately made to represent foam as a porous homogeneous mixture of air and sea water. Comparisons were made between theoretical and experimental (Hollinger 1971) brightness temperatures for identical

environmental conditions at 1.4 and 8.4 GHz. The results were excellent for vertical polarization and moderate for horizontal polarization."[3]

B. Conclusions

1. "The effects of sea water salinity on emissivities and brightness temperatures become negligible at frequencies above 4 GHz, for maximum salinity uncertainties of 4 parts per thousand."

The basis for this conclusion is a series of calculations of the emissivity of sea water for various salinities. The results of these calculations are shown in figure 1.

2. "Atmospheric contributions to specular ocean brightness temperatures are considerable, reaching a value of approximately 6°K for vertical polarization, a nadir angle of 45 degrees and clear sky conditions, at all frequencies from 1.4 to 9 GHz. The contribution is somewhat greater for heavier weather conditions. Thus, atmospheric effects must be treated with some care, if undue errors are to be avoided in derived surface temperatures."

This is a very important conclusion. There are glib remarks, from time to time, about the "all weather capability" of microwave radiometers. Certainly, atmospheric effects are small in the microwave region when compared with atmospheric effects in the infrared; however, it does not necessarily follow that atmospheric effects are negligible for microwave radiometers. Figures 2 and 3 illustrate the magnitude and frequency dependence of the problem.

3. "Ocean brightness temperatures show a maximum response to surface temperatures at a frequency of approximately 5 GHz, vertical polarization and a nadir angle of 60 degrees. For these conditions, the ratio of the change in brightness temperature to a given change in surface temperature is about 0.6 in the temperature interval 276-296°K."

One criterion for selecting a specific frequency or frequencies for sea surface temperature measurements is maximizing the change of brightness temperature for a corresponding change in physical temperature. Figure 4 shows change in brightness temperature for a given change in ocean physical temperature as a function of frequency, weather conditions, polarization, and incidence angle.

4. "Comparisons between theoretical and experimental rough surface brightness temperatures, without foam, show considerably better agreement for vertical polarization than for horizontal polarization. In the case of vertical polarization, all theoretical values fell within the experimental uncertainty."

An important part of any analytical effort is how well it can explain or predict measured quantities. A comparison with data taken by Hollinger (1970, 1971) is shown in figure 5. The data are restricted to lower wind speeds to avoid the difficulties associated with estimating the contribution of foam.

---

[3] Hollinger's data exclude foam effects; therefore, Porter and Wentz's foam model could not be compared with Hollinger's data.

5. "A foam layer may be realistically modeled as a random porous structure, consisting of 99% air and 1% sea water. The effects of multiple reflections in the foam layer should be taken into account in any future study. In this work, a simplified once-through radiative model, with a single reflection from the underlying water, provided a reasonable basis for determining the brightness temperatures of foam-covered ocean surfaces."

There is a shortage of measurements about both the physical properties (i.e., thickness, bubble size distribution, percentage composition, e.g., of water and air) of foam and its microwave emissivity. Nonetheless, if accurate sea surface temperature measurements with microwave radiometers are to be made, the effects of foam, when present, must be accounted for. Accordingly, the assumptions stated above were made; and calculations of the reflectivity, transmissivity, and emissivity were made for a multiple reflection model. A calculation made for a single reflection model was found to be in good agreement with the multiple reflection model. On the basis of this agreement, Porter and Wentz felt justified in using the single reflection model in their work in this report.

6. "Both horizontal and vertically polarized brightness temperatures of rough, foam-covered ocean surfaces are proportional to wind velocity, at frequencies from 1.4 to 5 GHz. In the case of vertical polarization, wind variations have a progressively smaller effect with increasing nadir angle until, in the vicinity of 60 degrees, brightness temperatures are almost independent of wind velocity. At vertical incidence, there is a gradual increase in brightness temperature sensitivity to wind velocity, at both polarizations, as frequency increases from 1.4 to 5 GHz."

Figure 6 shows the foam surface emission as a function of wind speed for selected frequencies. Figures 7 through 9 show computed brightness temperature as a function of incidence angle for various weather conditions.

7. "In a manner similar to the above, the brightness temperatures of rough, foam-covered ocean surfaces are proportional to atmospheric radiation, i.e., atmospheric moisture content. The effect is independent of polarization and nadir angle except at angles beyond 40 degrees, for the horizontal component of polarization, where a given increase in atmospheric moisture causes a somewhat greater increase in overall brightness temperatures. This is due to relatively higher surface reflectivities in this angular region. A change in atmospheric condition from Clear Sky to Heavy Rain, increases rough ocean brightness temperatures, at vertical incidence, by approximately 0.5°K at 1.4 GHz; 2°K at 2.5 GHz; 5°K at 4 GHz; and 8°K at 5 GHz."

Qualitatively, this is an obvious conclusion; however, the magnitudes of the numbers are equally significant and once again point up the importance of making a good atmospheric correction. Figures 7 and 9 show the atmospheric effects for 2.5 and 5.0 GHz, respectively.

8. "If the effects of atmospheric stability are neglected, an error of 0.8°K or less results in derived surface temperatures, at 2.5 GHz, for the operating and environmental conditions considered in the study."

Since waves develop more quickly and reach greater heights under conditions of atmospheric instability than they do for stable conditions, it was decided to consider the effects of atmospheric instability on sea-surface roughness and its effect on sea surface temperature determination. The results of that study are shown in table 1.

Table 1.--Effective wind speeds and corresponding brightness temperatures for wind speeds measured at 12.5 m and for various stability conditions (2.5 GHz, θ_0=60°, vertical polarization, clear sky, S=33°/$_{oo}$, T=284 K)

Wind speed measured at height of 12.5 m (m/s)	Effective wind speed (m/s)			Brightness temperature (K)		
	Stable	Cox & Munk*	Unstable	Stable	Cox & Munk*	Unstable
0	0	0	0	167.0	167.0	167.0
4	2.3	4	5.6	166.6	166.2	165.8
8	6.5	8	9.7	165.6	165.4	165.7
14	13.2	14	15.4	166.6	166.8	166.8
20	19.4	20	21.2	166.8	166.8	166.8

*(1954)

III. DISCUSSION OF "RESEARCH TO DEVELOP A MICROWAVE RADIOMETRIC OCEAN TEMPERATURE SENSING TECHNIQUE" (PORTER AND WENTZ 1972)

A. Summary

"The purpose of the research described in this report was to study in considerable detail the surface characteristics of the ocean to permit refinement of the microwave radiometric surface temperature sensing technique presented in Porter and Wentz (1971). The prime thrust of the current work involved the development of an analytical model, suitable for evaluating the effects of small-scale roughness attributable to capillary and short gravity waves. Concurrently, the effects of large-scale roughness were evaluated on the basis of a 2-dimensional geometric optics model furnished by Wagner (Lynch and Wagner 1972)."

In table 2 are the parameters forming the basis of the study.

"The ocean surface may be described as a statistically random rough surface. Accordingly, its electromagnetic reflection properties may be conveniently specified by its scattering characteristics. In this study, these have been divided into two categories:

1. Large-scale scattering, where the average roughness height is much larger than the radiation wavelength.

2. Small-scale scattering, where the average roughness height is much smaller than the radiation wavelength.

"Since the 2-dimensional model describing large-scale scattering is adequately described in Lynch and Wagner (1972) it is appropriate to mention the background for the small-scale scattering model developed in this study. The work of Rice (1951), which evolved from that of Lord Rayleigh, forms the basis for scattering by the small-scale component of rough surfaces. His theory, combined with the geometric optics approach to multiple scattering and shadowing, has yielded a composite model capable of furnishing bistatic scattering coefficients of reasonable accuracy. Any such model, however, is dependent on the availability of a suitable directional ocean wave spectrum. Fortunately, the work of Pierson (1972) has resulted in expressions that account for both the capillary and gravity wave spectrum; these have been used to advantage in this study.

Table 2.--Parameters forming the basis of the work by Porter and Wentz (1972)

Frequencies:	2.5, 3.5, and 5 GHz		
Polarization:	Vertical (horizontal polarization taken into account with regard to scattering)		
Nadir Angles:	0° to 60°		
Temperatures:	Surface		Atmosphere (near surface)
	Unstable conditions	Stable conditions	
	272 K	---	265 K
	291	285	288
	302	296	298
Salinities:	31, 34, and 37°/$_{oo}$		
Wind velocities:	4, 8, 14, and 20 m/s		
Latitudes:	Tropical, middle-latitude, and subpolar		
Atmospheric models (10 in all):	Clear sky Cloud Moderate rain--6 mm/hr Heavy rain--15 mm/hr		
Foam model:	Incorporating effects of whitecaps and foam streaks		
Spray model:	Wind-driven spray, based on laboratory investigations		

"A considerable amount of attention has been given to improvement of the previous foam model. As a result of recent experimental data generated by Ross (1972) and Williams (1971) it was possible to utilize a more appropriate model, consisting of whitecaps and wind-driven foam streaks, with somewhat more realistic values of microwave emissivities assigned to these components."

B. Conclusions

(In the ensuing discussion, SSS is small-scale scattering and LSS is large-scale scattering.)

1. "SSS coefficients have a broader angular distribution, especially at large incidence angles, than LSS coefficients. In the specular direction, LSS dominates; however, at angles far removed from the specular, SSS becomes the dominating mechanism. At non-zero incidence angles, SSS appears to be an effective backscatterer."

Figures 10 and 11 show the small-scale scattering coefficients as a function of zenith scattering angle for incidence angles of 0° and 60° and a frequency of 2.5 GHz. Figures 12 and 13 show the large-scale scattering coefficients for the same set of variables. By comparing figures 10 and 12 and figures 11 and 13, the differences in angular variation of the LSS coefficients and the SSS coefficients are readily apparent.

2."The most significant effect of SSS on brightness temperatures is the reduction of rms slopes characterizing LSS. This tends to make the surface appear more specular than is the case when unmodified slopes are used."

At first glance, this appears contradictory to conclusion 1; however, examination of figures 10 through 13 shows that the SSS is an order of magnitude smaller than the LSS for angles near specular reflection. Thus near the specular point, scattering is dominated by the LSS component. Conservation of energy requires that energy used to generate SSS is not available to generate LSS; therefore, the inclusion of SSS tends to make the surface more specular. This can be seen in figure 14, which is a plot of emissivity versus nadir angle for identical conditions with the old (Porter and Wentz 1971) and new (Porter and Wentz 1972) models.

3."The composite scattering coefficient, Γ^c, is a function of salinity, S, and water temperature, T_w, only through the complex dielectric permittivity, ε. The dependence is small, and variations in Γ^c, caused by changing T_w and S, can be approximated by the corresponding specular reflectivity variation, with only a 0.1% error resulting for the ranges considered in the study."

The validity of this statement can be seen by first noting the form of the expression for the composite scattering coefficient as given in section 2 of Porter and Wentz (1972) and then the equations for the complex dielectric permittivity as given in section 2 of Porter and Wentz (1971). As examples, consider the cases where: (1) all conditions are the same except that the salinities are 31°/$_{oo}$ and 34°/$_{oo}$ and (2) all conditions are the same except that the water temperatures are 285.2 K and 291.2 K.

Case 1. For a salinity of 31°/$_{oo}$, the specular and rough emissivities are 0.3453 and 0.3445, respectively. For a salinity of 34°/$_{oo}$, the specular and rough emissivities are 0.3435 and 0.3422, respectively. The ratio $(SE)_{31}/(SE)_{34}$=0.3453/0.3435=1.00524, and the ratio $(RE)_{31}/(RE)_{34}$=0.3445/0.3422=1.00672 so that (1.00672-1.00524)/1.00672=0.0015 or the error is about 0.05%/°/$_{oo}$ (percent per part per thousand).

Case 2. For a surface temperature of 285.2 K, the specular and rough emissivities are 0.3469 and 0.3449, respectively. For a sea-surface temperature of 291.2 K, the specular and rough emissivities are 0.3458 and 0.3425, respectively. (The rough emissivities have had the foam contribution removed.) The ratio $(SE)_{285.2}/(SE)_{291.2}$=0.3469/0.3458=1.0032, and the ratio $(RE)_{288.2}/(RE)_{291.2}$=0.3449/0.3425=1.0070 or (1.0070-1.0032)/1.0070=0.06%/K (percent per degree Kelvin).

4. "It was determined that the scattering model conserved energy within 5%. Following the imposition of a normalizing condition, this error was reduced to 1.5%. Comparisons with Hollinger's measurements, at θ_0=40°, showed an rms deviation between derived and measured brightness temperatures of 2.0%, i.e., 2.7°K. This figure was taken to be the upper bound on modeling error, due to the relatively high experimental error. Comparisons at angles, in the range 40°<θ_0<60°, showed good agreement. The disagreement, at small angles, may be due to antenna pattern effects."

During the course of lengthy, involved numerical calculations, it is often necessary to have "check points." A very convenient one for scattering calculations is the conservation of energy. For a perfect conductor, the integrated reflection should be one,and the integrated emissivity should be zero. Computations were performed for incidence angles of 0°, 30°, and 60°. To impose an additional normalizing condition to reduce the error to an acceptable level was necessary.

Figures 15 and 16 show comparisons with data taken by Hollinger (1971). The agreement between measurement and calculation is quite good particularly between 30° and 60° incidence angle.

5."Sea spray does not contribute significantly to over-all brightness temperatures, nor does it significantly attenuate radiation emanating from the surface."

Measurements by Shemdin (1972) of the size distribution and mass density of sea-spray droplets indicate most droplets are 1 mm or less in diameter and have a mass density of 10^{-1} g/m^2 or less. Since $(2\pi r)/\lambda \simeq 10^{-1}$ for 5 GHz, Rayleigh scattering can be applied. Under the above assumptions, the computed attenuation is on the order of 10^{-6}.

6."Over-all brightness temperatures are slightly affected by fetch direction. Brightness temperatures, for the crosswind situation, are smaller than for the upwind case, out to $\theta_0=60°$, with a maximum difference of about 1°K occurring at intermediate incidence angles, $30°<\theta_0<50°$."

Figure 17 shows a plot of the small difference between the computed upwind brightness temperature and the computed crosswind brightness temperature.

7."At small incidence angles, a rougher sea appears warmer for vertical polarization because (1) tilting of the surface elements results in larger emission angles and (2) the generation of foam increases the over-all surface emissivity. For $40°<\theta_0<50°$, the brightness temperature curves cross over because the clear rough emissivity increases with angle at a slower rate than the specular emissivity, while the foam emissivity, for vertical polarization, decreases with angle[4] out to about 60°. A crossover angle of $\theta_0=43°$ appears to be optimum for a surface temperature sensing application because of the elimination of roughness effects at this angle."

Figures 18 and 19 show brightness temperature versus incidence angle for a variety of wind speeds. As can be seen, for smaller incidence angles a rougher sea appears warmer. Another very interesting feature of these figures is the crossing region between $40°<\theta_0<50°$, indicating a region where the emissivity is minimally dependent on roughness.

A comparison of figures 18 and 19 with figures 7 through 9 shows that the region of minimum dependence of emissivity on roughness has shifted significantly from a value near 60° to

[4]The basis for this statement is Stogryn (1972).

about 43°. This probably is due to refinements in the model for foam emissivity and the inclusion of small-scale scattering.

8. "Uncertainties in water temperature sensing, ΔT_W, caused by salinity uncertainties, Δs, decrease with increasing frequency. Water temperature sensing uncertainties, caused by brightness temperature uncertainties, ΔT_B, also decrease with increasing frequency, in the 2.5-5.0 GHz range. However, ΔT_W increases with frequency for atmospheric uncertainty, $\Delta\alpha$. Assuming realistic uncertainties, the combined effect of these terms establishes an optimum frequency in the range 3.0±0.5 GHz, for surface temperature sensing."

Figure 20 shows the uncertainty in brightness temperature for an uncertainty in salinity for a specified set of environmental conditions.

Figure 21 shows dT_W/dT_B as a function of frequency. This figure reflects the increase in emissivity of sea water with frequency.

Figure 22 shows $dT_B/d\alpha$ (α is atmospheric attenuation) as a function of frequency for three weather conditions.

9. "To derive water temperatures within ±1.5°K and ±1.0°K, with a perfectly calibrated noise-free radiometer, with no modeling error, the environmental uncertainties, namely, windspeed, wind direction, atmospheric condition and salinity, must not exceed 15% and 10%, respectively, of the total variation that occurs in the natural environment."

Table 3 shows the effect of uncertainty in atmospheric attenuation near the optimum frequency. ($\Delta\phi_0$ is the uncertainty in wind direction.)

Table 3.--Effect of atmospheric uncertainty on optimum frequency

Atmospheric uncertainty, $\Delta\alpha$, millinepers	Water temperature uncertainty, ΔT_W, K	
	f=2.5 GHz	f=3.5 GHZ
1	1.7	2.0
0.6	1.5	1.5
0.5	1.5	1.2

ΔU=2 m/s, ΔS=1°/$_{oo}$, $\Delta\phi_0$ = 10°
Middle-latitude, clear sky

Table 4 shows uncertainties in wind speed, salinity, and atmospheric attenuation for which derived water temperatures are ±1.5 K and ±1 K. These calculations do not consider radiometer noise or calibration uncertainties, although figure 21 could be used to do so. It is

Table 4.--Uncertainties under which $\Delta T_W = \pm 1.5$ K and ± 1.0 K can be realized for f^{0p} and θ_0^{0p}

$\Delta T_W = \pm 1.5$ K
$\Delta U_{max} = \pm 3.8$ m/s,
$\Delta s_{max} = \pm 7.5°/_{oo}$,
$\Delta \alpha_{max} = \pm 1.6$ millineper,
or $\{\Delta U = \pm 2$ m/s, $\Delta S = \pm 1°/_{oo}$, $\Delta \alpha = \pm 0.6$ millinepers$\}$.
$\Delta T_W = \pm 1.0$ K
$\Delta U_{max} = \pm 2.5$ m/s,
$\Delta S_{max} = \pm 5.0°/_{oo}$,
$\Delta \alpha_{max} = \pm 1.1$ millineper,
or $\{\Delta U = \pm 1.3$ m/s, $\Delta s = \pm 0.7°/_{oo}$, $\Delta \alpha = \pm 0.4$ millinepers$\}$.

also interesting to note that the effect of considering radiometric uncertainties is to make the optimum frequency somewhat higher.

Figure 22 and table 3 show the significance of uncertainties in atmospheric attenuation.

IV. DISCUSSION OF "THE EFFECT OF SURFACE ROUGHNESS ON MICROWAVE SEA BRIGHTNESS TEMPERATURES" (WENTZ 1974)

A. Summary

"Microwave radiometric remote sensing of sea temperature to within ±1°K, and local surface wind speed to within ±2 m/s, will require the generation of sophisticated hardware and software. Whenever possible, the software should be firmly based on the physics of the problem and should not rely primarily on empirically derived relationships. For theoretical models to be capable of predicting sea brightness temperatures in accordance with the above tolerances, a large number of environmental factors must be considered. The aim of this study was to evaluate one such factor: sea surface roughness. Earlier studies (Porter and Wentz 1971) and (Porter and Wentz 1972) established the need for considering surface irregularities, both large and small compared to the radiation wavelength, as well as the foam riding on the sea surface. The effect of such roughnesses on microwave sea brightness temperatures is the subject of this report.

"The objectives of this study were:

1. To develop a two-scale scattering model that accounts for surface irregularities, both large and small compared to the radiation wavelength, and that complies with the conservation of energy.

2. To evaluate the wind dependence of foam-free sea brightness temperatures.

3. To investigate the effect of wind duration on the two-scale scattering model.

4. To suggest a technique for remotely sensing sea water temperature and local surface wind speed utilizing both the horizontal and vertical components of brightness temperature.

5. To investigate scattering from sea foam and to make relevant comparisons with experimental data."

The following paragraph is offered in summary without additional documentation.

"Rice's (1951) perturbation theory, describing scattering from surface irregularities that are small compared to the radiation wavelength, has been combined with geometric optics to yield a two-scale scattering theory which conserves energy. The relationship, in the limit of perfect conductivity, between Peake's small-scale scattering coefficients (Peake and Barrick 1967) and Wu and Fung's (1972) modified reflection coefficients, ensures that energy is exactly conserved to the second order in the perturbation parameter $k\zeta_s$ (k=radiation wave-number, ζ_s=small-scale rms height)."

B. Conclusions

1. "Sea surface computations, based on a large-scale, ray-tracing model, which randomly samples the distribution of large-scale intersection slopes, and computations based on the Wagner and Lynch (1972) geometric-optics model, which integrates over the distribution of slopes, agree for incidence angles less than 60°. The small disagreement, seen at larger incidence angles, probably results from the different manner in which the two models treat shadowing and multiple reflections."

Figure 23 shows a comparison between emissivities as computed by Wentz (1974) and Wagner and Lynch (1972). The solid curves are the emissivities calculated by Wentz (1974) and the x's are computations based on the Wagner and Lynch (1972) geometric-optics model. Neither calculation considers the effects of foam.

2. "Pierson and Stacy's (1973) sea spectrum is divided into large and small-scale components. The division point is called the cutoff wave-number K_c. The computed sea brightness temperatures are fairly insensitive to the choice of K_c, particularly at 1.41 GHz, provided that the perturbation parameter $k\zeta_s$ is within the range 0.125 to 0.25."

Figure 24 shows the change in emissivity as a function of the cutoff wave number. The X and O points are for a perturbation parameter 0.125 and 0.25, respectively. The data actually are plotted as the ratio of the cutoff wave number to the radiation wave number. This permits comparison of the different frequencies, as the cutoff wave number is a function of the radiation wave number.

3. "Brightness temperatures, T_B, are computed from the two-scale scattering model and from the geometric-optics model, as a function of incidence angle. Comparisons are made with experimental data (Hollinger 1971) at 1.41, 8.36, and 19.34 GHz. In all cases, the angular behavior of the two-scale T_B is more in accord with experimental data, than is the behavior of the geometric-optics T_B."

Figures 25 through 27 show data taken by Hollinger (1971) at 1.41, 8.36, and 19.34 GHz for horizontal and vertical polarization as a function of incidence angle. The circles and

crosses are average measurements for wind speeds of 0.5 and 13.5 m/s, respectively. The solid curves (labeled $k\zeta_s$=0.25) show the computed brightness temperature for the two-scale model for a wind speed of 13.5 m/s. The large dashed curves (labeled $k\zeta_s$=0) show the large-scale geometric optics brightness temperatures for a wind speed of 13.5 m/s. The small dashed curves (labeled specular and corresponding to $k\zeta_s$=0 and σ=0) correspond to the 0.5 m/s data.

4. "The two-scale T_B versus wind speed dependence is approximately linear, for incidence angles less than 55° except at 19.34 GHz, at which the high downward sky brightness temperature adds some curvature to the dependence."

Figures 28 through 30 show brightness temperature versus wind speed for 1.41, 8.36, and 19.34 GHz. The dashed curves, labeled measurement, are from Hollinger (1971). It is interesting to note the flatness of measured brightness temperatures at 55° incidence angle and vertical polarization at all frequencies. Also interesting to note is the increase of calculated brightness at nadir as wind increases for the small-scale model. This was not explained by previous theory. Foam has been ignored.

5. "The slope of the two-scale T_B wind dependence is in better agreement with measurements than is the slope computed from the geometric-optics model. At nadir, the two-scale T_B shows a larger wind dependence, and at large incidence angles, it shows a smaller dependence."

Figure 31 shows $\Delta T/\Delta U$ versus incidence angle for horizontal polarization and the three frequencies of interest. Similarly, figure 32 shows this information for vertical polarization. The $k\zeta_s$=0 corresponds to the geometric optics case. The dashed lines show limits on the range of experimental values measured and calculated by Hollinger (1971). The solid curves are the theoretical values computed from the two-scale model.

Note that, for horizontal polarization, the geometric optics model shows a much steeper slope than either the models with small-scale scattering or the experimental data. For the vertical polarization, note that the zero crossing (i.e., the point of no sensitivity to wind speed) is moved to larger incidence angles by the inclusion of small-scale scattering.

6. "The best-fit between the two-scale T_B wind dependence and the experimental dependence would result from reducing the large-scale slope variance, probably by 1/4 to 1/3."

In this study, Wentz (1974) uses the wave spectrum reported by Pierson and Stacy (1973). The value of σ^2 (the large-scale slope variance) reported by Pierson and Stacy (1973) is significantly larger than the one reported by Cox and Munk (1954).

7. "Best agreement in wind dependence occurs at 1.41 GHz, at which the two-scale model gives substantially better results than the geometric-optics model. Excellent agreement is shown for the percentage polarization X, which possibly results from X being insensitive to absolute calibration errors and to variations in sea salinity, water temperature, and atmospheric conditions."

Figure 33 shows change of polarization with change in wind speed, $\Delta X/\Delta U$, versus incidence angle for the three frequencies used by Hollinger (1971) in his measurement. Percentage polarization is defined as the ratio of the difference between the horizontal and vertical intensities divided by their sum.

8. "Based on the assumptions that, initially, the sea salinity is known to within $\pm 1°/_{oo}$, the sea water temperature is known to within $\pm 10°K$ and the wind speed is between 0 to 10 m/s; the model developed in this study predicts that a system, which utilizes a dual frequency (2.7 and 9.3 GHz) radiometer capable of measuring brightness temperature with no error can determine sea water temperature to within $\pm 1°K$ and the local surface wind speed to within ± 1.5 m/s, regardless of atmospheric conditions. Environmental parameters not considered in the model, such as foam, sun glitter, and small-scale anisotropy, may, of course, increase the sensing errors."

This is an extremely important conclusion even with the restrictions noted above. Accordingly, Wentz (1974) gives the method as follows. In this topic, U=wind speed in m/s, $T_B^V(f)$= brightness temperature for vertical polarization at frequency f, $\Xi \equiv T_B^V(9.3) - T_B^V(2.7)$, S= salinity, T_W=water temperature, X=percent polarization, and α=atmospheric attenuation.

"A possible water temperature and roughness sensing technique will now be sketched out, based on the following assumptions:

1. Geographical and temporal variations in sea salinity are known to within $\pm 1°/_{oo}$.

2. The water temperature is initially known to within $\pm 10°K$.

3. The wind speed is between 0 and 10 m/s. The calculations in this section are based on a foam-free brightness temperature model, and the upper limit on wind speed is required to insure that the foam effects on brightness temperatures will be small (Porter and Wentz 1972).

"A dual-frequency, 2.7-9.3 GHz, radiometer is employed. the nadir angle of the radiometer antenna beam is such that $\theta_0 = 43°$. Measurements of the horizontally and vertically polarized components of brightness temperature are taken at 2.7 GHz, and the vertical brightness temperature is measured at 9.3 GHz, to allow correction for atmospheric effects.

"The difference Ξ between T_B^V, measured at 9.3 GHz and 2.7 GHz, is a very good indicator of atmospheric attenuation, as shown in table 5. The changes in Ξ, per unit change in salinity, water temperature, and atmospheric attenuation were calculated assuming a specular surface. These variations should not change appreciably as a function of roughness. The wind speed variation, in table 5, was approximated by the difference between $\Delta T_B^V/\Delta U$, given in figure 32 at 8.36 GHz and 1.41 GHz. The atmospheric attenuation refers to the attenuation measured at 2.7 GHz. For the assumed uncertainties, $\Delta S = \pm 1°/_{oo}$, $\Delta T_W = \pm 10°K$, and $\Delta U = \pm 5$ m/s, the total variation in Ξ can be calculated from table 5.

$$\Delta\Xi = \left\{ \left[\left(\frac{d\Xi}{dS} \right)^2 \Delta S \right]^2 + \left[\left(\frac{d\Xi}{dT_W} \right) \Delta T_W \right]^2 + \left[\left(\frac{d\Xi}{dU} \right) \Delta U \right]^2 \right\}^{1/2}, \text{ or } \Delta\Xi \simeq \pm 1.2°K \qquad (1)$$

where the uncertainties are assumed uncorrelated.

Table 5.--Variations in the difference of vertical brightness temperatures at 9.3 GHz and 2.7 GHz

$d\Xi/dS$	0.4 K/(°/$_{oo}$)
$d\Xi/dT_W$	0.1
$d\Xi/d\alpha$	8 K/millineper
$d\Xi/dU$	0.1 K/m/s

"In comparison with this ±1.2°K variation, Ξ increases by about 30°K when the atmosphere changes from clear sky to heavy rain, Ξ, thus, provides a very good measure of atmospheric attenuation and can be used to determine α, to within an uncertainty $\Delta\alpha$, resulting from the assumed uncertainties in S, T_W, and U. That is,

$$\Delta\alpha=(d\Xi/d\alpha)^{-1}\Delta\Xi\simeq\pm 0.15 \text{ millinepers.} \qquad (2)$$

Once Ξ has been measured, and α determined to within ±0.15 millinepers, the surface roughness may be determined by measuring the percentage polarization, X, at 2.7 GHz. The variation in X, due to the parametric uncertainties other than wind speed, is given by

$$\Delta X=\left\{\left[\left(\frac{dX}{dS}\right)\Delta S\right]^2+\left[\left(\frac{dX}{dT_W}\right)\Delta T_W\right]^2+\left[\left(\frac{dX}{d\alpha}\right)\Delta\alpha\right]^2\right\}^{1/2} \qquad \Delta X\simeq\pm 0.1\% . \qquad (3)$$

The measurement of X can then be used to determine surface roughness to within an uncertainty ΔU resulting from the uncertainties in S, T_W, and α.

$$\Delta U=\left(\frac{dX}{dU}\right)^{-1}\Delta X \qquad \Delta U\simeq\pm 0.7 \text{ m/s.} \qquad (4)$$

"This means that surface roughness can be determined within variations corresponding to a ±0.7 m/s change in wind speed. It does not mean that the wind speed can be determined to within ±0.7 m/s because it is not possible to distinguish between the effects of wind speed, direction, duration and atmospheric stability. However, X should be a good indicator of surface wind speed,[5] which is insensitive to atmospheric stability. Assuming that the duration and directional effects do not contribute more than a factor of 2 to the uncertainty, which seems unrealistic, a measurement of X would determine the local surface wind speed to within a ±1.5 m/s uncertainty.

"Turning now to the determination of water temperature, the variation in T_B^V due to the parametric uncertainties, other than water temperature, is given by an expression analogous to (1) and (3).

$$\Delta T_B^V=\left\{\left[\left(\frac{dT_B^V}{dS}\right)\Delta S\right]^2+\left[\left(\frac{dT_B^V}{d\alpha}\right)\Delta\alpha\right]^2+\left[\left(\frac{dT_B^V}{dU}\right)\Delta U\right]^2\right\}^{1/2} \qquad (5)$$

where ΔU comes from (4) and the values of the differentials are the maximum values given in Table 3-2[6] for 2.5 GHz. The salinity uncertainty is the dominating term in (5) and is responsible for most of the 0.4°K uncertainty. The corresponding uncertainty in water temperature is

$$\Delta T_W=(dT_W/dT_B^V)\Delta T_B^V\simeq\pm 1\text{°K} \qquad (6)$$

where the differential is taken from Table 3-2[6] for 2.5 GHz at mid-latitude.

[5]Or surface wind stress

[4]Not included in this summary

"In summary, based on the assumptions that, initially, the sea salinity is known to within $\pm 1^{\circ}/_{oo}$, the sea water temperature is known to within $\pm 10^{\circ}K$ and the wind speed is between 0 and 10 m/s; the model developed in this study predicts that a system, which utilizes a dual frequency (2.7 and 9.3 GHz) radiometer capable of measuring brightness temperature with no error can determine sea water temperature to within $\pm 1^{\circ}K$ and the local surface wind speed to within ± 1.5 m/s, regardless of atmospheric conditions.

"The above stated uncertainties represent a substantial reduction in the initially assumed uncertainties of $T_W = \pm 10^{\circ}K$ and $U = \pm 5$ m/s. An iteration could be performed using these smaller uncertainties as the initial values, and ΔT_W and ΔU could be reduced even more. To accurately determine the extent to which the uncertainties could be reduced, a more complete parametric analysis is required."

9. "Theoretical computations used on an air-foam-water layered structure and on a two-scale 100%-foam-covered surface do not agree with the vertically polarized, foam emissivity versus incidence angle dependence reported by Stogryn (1972)."

Figures 34 and 35 show the emissivity of foam versus incidence angle for 2.65 and 13.4 GHz, respectively. The curves labeled empirical are after Stogryn (1972). In the 2.65-GHz case, the horizontal polarization curves all show the same basic shape although the absolute magnitudes are different. In the vertical polarization case, not only are the absolute magnitudes different, but also the basic shapes of the curves are quite different. The empirical curves show a decrease in emissivity with increasing incidence, whereas the theoretical curves show an increase. For the 13.4-GHz case, the disagreement between the empirical and theoretical values is complete. Although two thicknesses bracket the empirical in magnitude at nadir, the angular dependence of the theoretical and empirical curves is exactly opposite. Note that Stogryn's empirically derived values are based on a rather limited data set with considerable scatter in the set. Thus, probably the best conclusion to draw is that a great deal of experimental and theoretical work must be done on the problem of the microwave emissivity of foam.

ADKNOWLEDGMENTS

The author wishes to acknowledge the encouragement and editorial assistance of Alan Strong, particularly during the early phases of the writing of this technical memorandum. The author would like to take this opportunity to express his regards to Ron Porter and Frank Wentz for the quality and quantity of their work under the NOAA contracts. Finally, the author would like to acknowledge the NESS Design and Drafting Group for drafting the multitudinous figures appearing in this technical memorandum.

REFERENCES

Cox, C., and Munk, W., "Statistics of the Sea Surface Derived From Sun Glitter," Journal of Marine Research, Vol. 13, No. 2, Nov. 1954, pp. 198-227.

Hollinger, James P., "Passive Microwave Measurements of the Sea Surface," Journal of Geophysical Research, Vol. 75, No. 27, Sept. 27, 1970, pp. 5209-5213.

Hollinger, James P., "Passive Microwave Measurements of Sea Surface Roughness," IEEE Transactions on Geoscience Electronics, Vol. GE-9, No. 3, July 1971, pp. 165-169.

Lynch, P.J., and Wagner, R.J., "Rough Surface Scattering: Shadowing Multiple Scatter and Energy Conservation," Journal of Mathematical Physics, Vol. 11, No. 10, Oct. 1970, pp. 3032-3042.

Lynch, P.J., and Wagner, R.J., "Emission and Reflection From Anisotropic Random Rough Surfaces," Technical Report 17608-6005-RO-00, prepared for the Office of Naval Research, Washington, D.C., by the TRW Systems Group, Redondo Beach, Calif., Mar. 1972, 62 pp.

Peake, W.H., and Barrick, D.E., "Scattering From Surfaces With Different Roughness Scales: Analysis and Interpretation," Research Report BAT-197A-10-3, Battelle Memorial Institute, Columbus, Ohio, Nov. 1967, 63 pp.

Pierson, W.J. (University Institute of Oceanography, City University of New York, N.Y.), June 1972 (personal communication).

Pierson, W.J., and Stacy, R.A., "The Elevation, Slope, and Curvature Spectra of a Wind Roughened Sea," Contractor Report NASA CR-2247, National Aeronautics and Space Administration Langley Research Center, Hampton, Va., Dec. 1973, 125 pp.

Porter, R.A., and Wentz, F.J., III, "Microwave Radiometric Study of Ocean Surface Characteristics," Final Report, 2 vols., NOAA (National Oceanic and Atmospheric Administration) Contract No. 1-35140, Radiometric Technology, Inc., Wakefield, Mass., July 1971, 275 pp. and 377 pp.

Porter, R.A., and Wentz, F.J., III, "Research To Develop a Microwave Radiometric Ocean Temperature Sensing Technique," Final Report, 2 vols., NOAA (National Oceanic and Atmospheric Administration) Contract No. 2-35309, Radiometric Technology, Inc., Wakefield, Mass., Dec. 1972, 150 pp. and 216 pp.

Rice, S.O., "Reflection of Electromagnetic Waves From Slightly Rough Surfaces," Communications in Pure and Applied Mathematics, Vol. 4, No. 2/3, Aug. 1951, pp. 351-378.

Ross, D.B. (Atlantic Oceanographic and Meteorological Laboratory, National Oceanic and Atmospheric Administration, U.S. Department of Commerce, Virginia Key, Miami, Fla.), 1972 (personal communication).

Shemdin, O. (Department of Coastal and Oceanographic Engineering, University of Florida, Gainesville), Feb. 1972 (personal communication).

Stogryn, A., "The Emissivity of Sea Foam at Microwave Frequencies," Journal of Geophysical Research, Vol. 77, No. 9, Mar. 20, 1972, pp. 1658-1666.

Wagner, R.J., and Lynch, P.J., "Analytical Studies of Scattering and Emission by the Sea Surface," Technical Report 17608-6006-RO-00, prepared for the Office of Naval Research, Washington, D.C., by the TRW Systems Group, Redondo Beach, Calif., Mar. 1972, 63 pp.

Wentz, F.J., III, "The Effect of Surface Roughness on Microwave Sea Brightness Temperatures," Final Report, NOAA (National Oceanic and Atmospheric Administration) Contract No. 3-5345, Radiometric Technology, Inc., Wakefield, Mass., Mar. 1974, 97 pp.

Williams, G.F., Jr., "Microwave Emissivity Measurements of Bubbles and Foam," IEEE Transactions on Geoscience Electronics, Vol. GE-9, No. 4, Oct. 1971, pp. 221-224.

Wu, S.T., and Fung, A.K., "A Noncoherent Model for Microwave Emissions and Backscattering From the Sea Surface," Journal of Geophysical Research, Vol. 77, No. 30, Oct. 20, 1972, pp. 5917-5929.

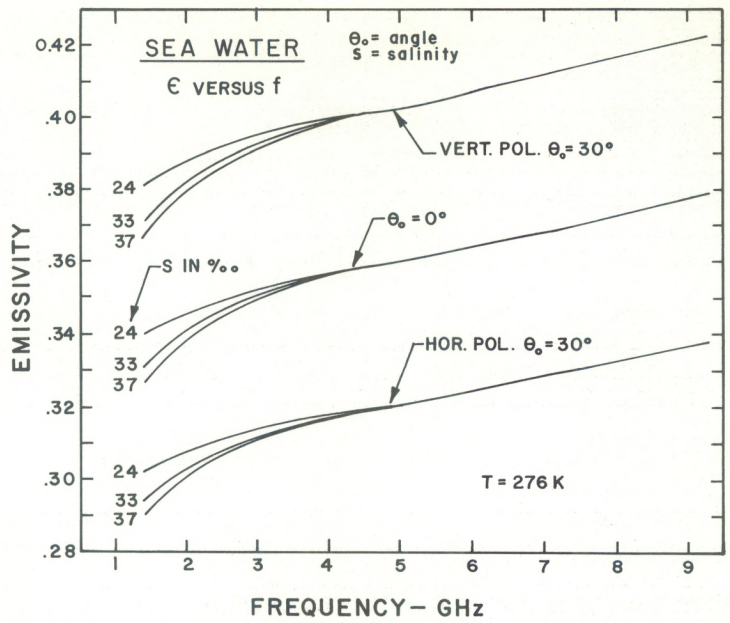

Figure 1.--Specular emissivity of model sea water versus frequency for T=276 K. Vertical polarization is VERT. POL., and horizontal is HOR.

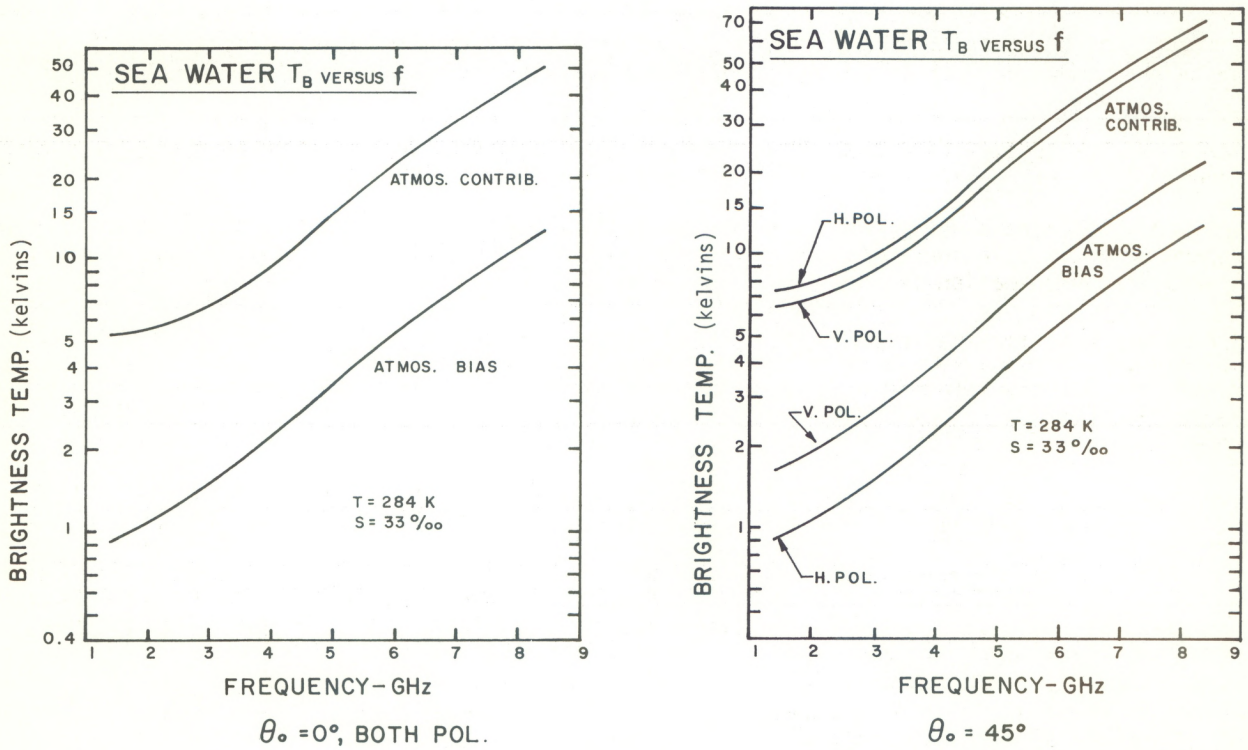

Figure 2.--Atmospheric contribution to specular brightness temperatures, as a function of frequency (clear sky, T=284 K, S=33°/₀₀) for incidence angles, θ_0, of 0° and 45°. Vertical polarization is V. Pol., and horizontal is H.

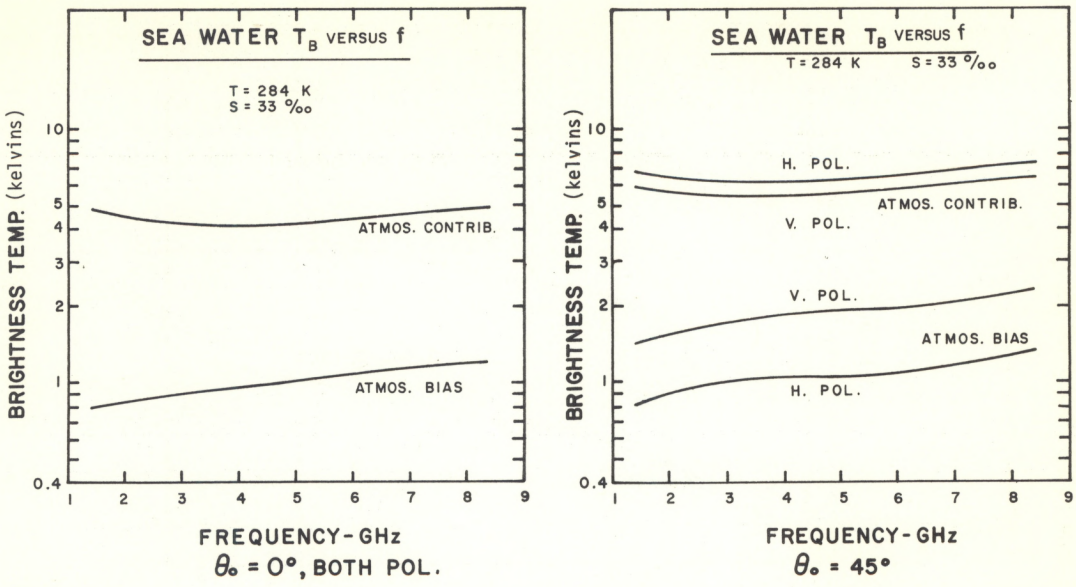

Figure 3.--Atmospheric contribution to specular brightness temperatures, as a function of frequency (heavy rain, T=284 K, S=33°/₀₀) for incidence angles, θ_0, of 0° and 45°

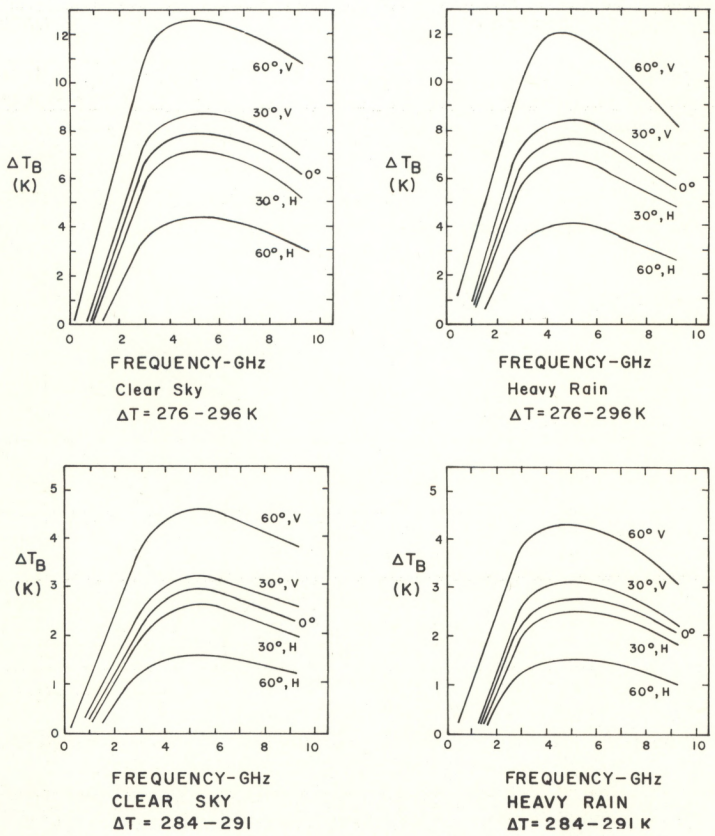

Figure 4.--Specular brightness temperature response to changes in surface temperature, as a function of frequency (S=33°/₀₀) for various incidence angles. V is vertical polarization, and H is horizontal polarization.

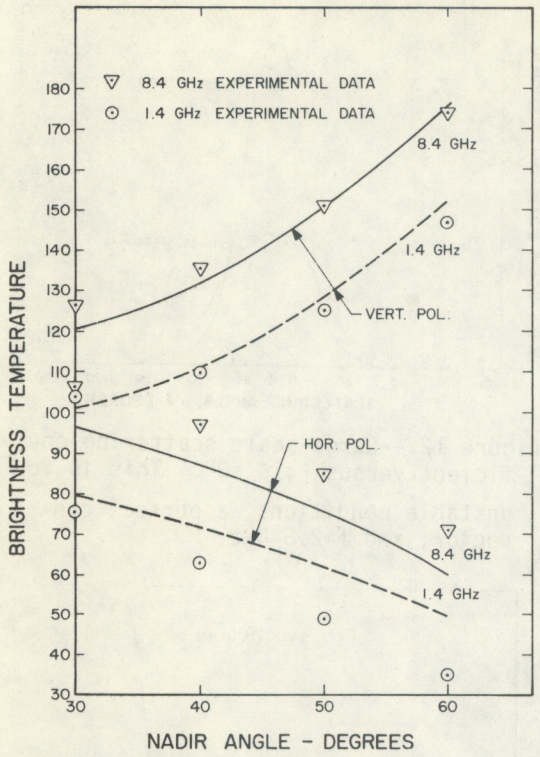

Figure 5.--Comparison of theoretical and experimental ocean brightness temperatures in kelvins for wind speed U=0 m/s and f=1.4 and 8.4 GHz

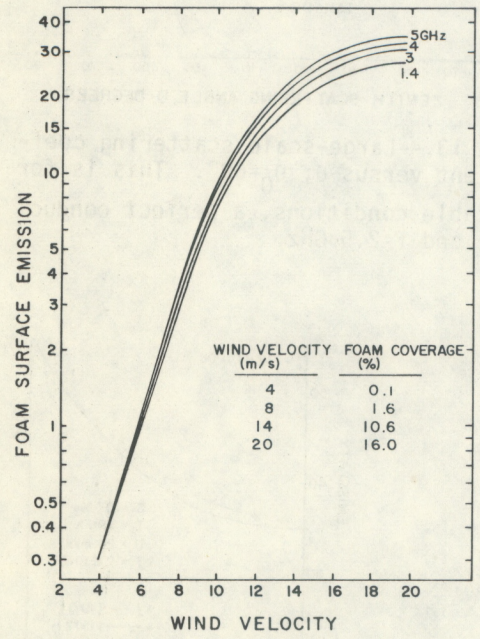

Figure 6.--Foam surface emission in kelvins versus wind velocity in meters per second for various frequencies (T=284 K, θ_0=0°, S=33°/$_{oo}$, clear sky). The foam thickness is 1.7 cm.

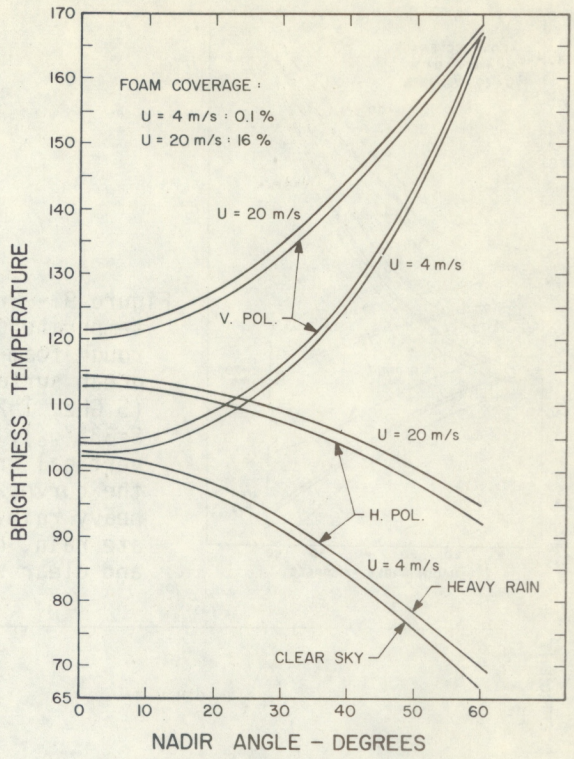

Figure 7.--Brightness temperatures in kelvins of rough foam-covered ocean surfaces (2.5 GHz, T=284 K, S=33°/$_{oo}$)

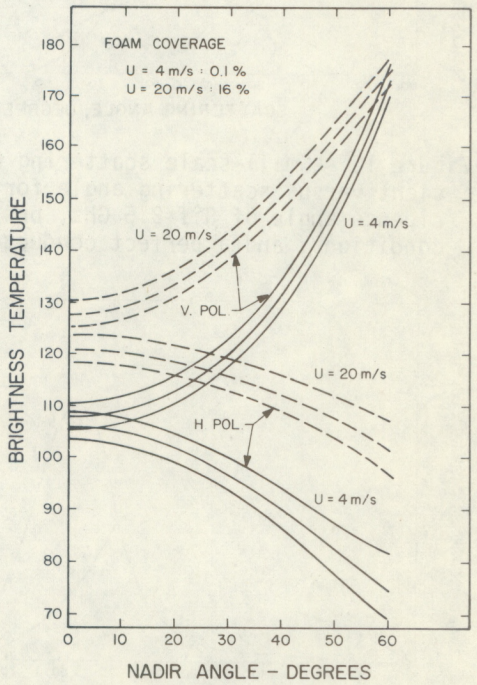

Figure 8.--Brightness temperatures of rough foam-covered ocean surface (4 GHz, T=284 K, S=33°/$_{oo}$). The curves are in vertical order: heavy rain, moderate rain, and clear sky.

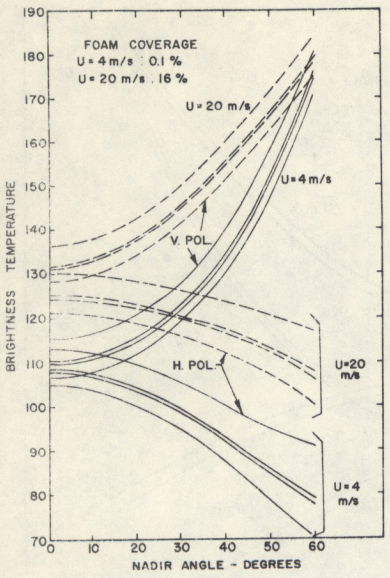

Figure 9.--Brightness temperatures of rough foam-covered ocean surface (5 GHz, T=284 K, S=33°/₀₀). The vertical order of the curves is heavy rain, moderate rain, cloud, and clear sky.

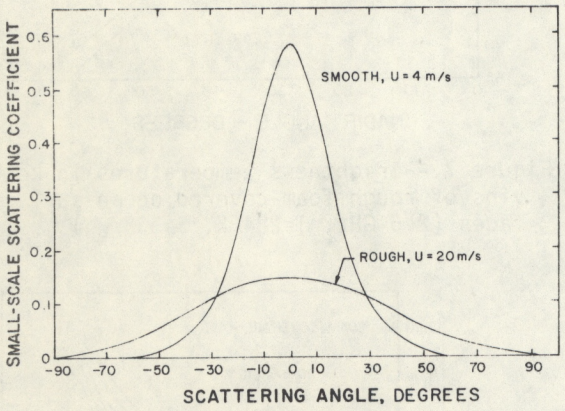

Figure 10.--Small-scale scattering coefficient versus scattering angle for an incidence angle of 0°f=2.5 GHz, unstable conditions, and a perfect conductor

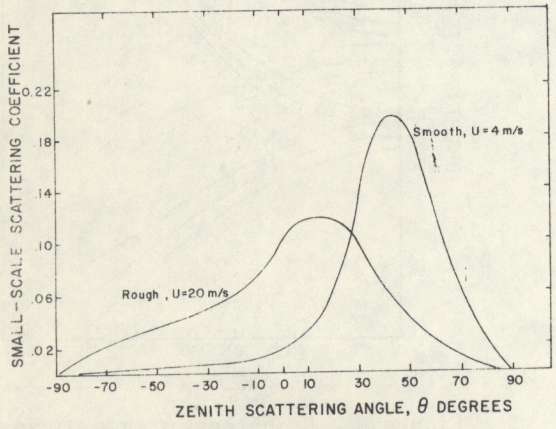

Figure 11.--Small-scale scattering coefficient versus θ; θ_0=60°. This is for unstable conditions, perfect conductor, and f°=2.5 GHz.

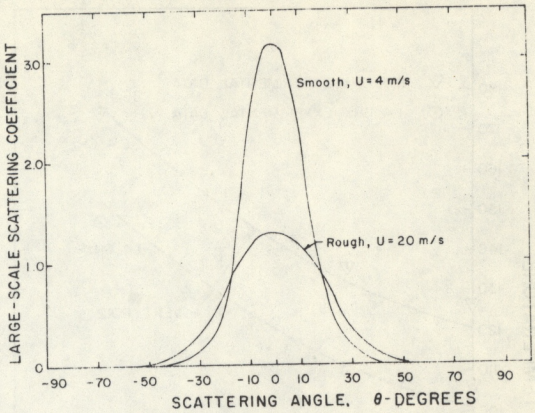

Figure 12.--Large-scale scattering coefficient versus θ; θ_0=0°. This is for unstable conditions, a perfect conductor, and f=2.5 GHz.

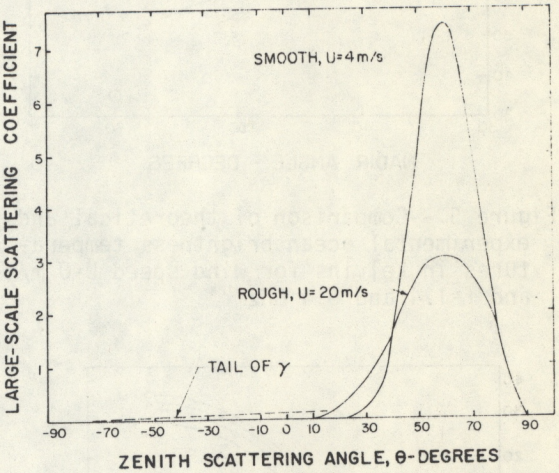

Figure 13.--Large-scale scattering coefficient versus θ; θ_0=60°. This is for unstable conditions, a perfect conductor, and f=2.5 GHz.

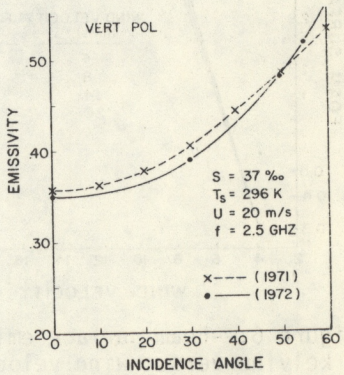

Figure 14.--Emissivity versus incidence angle for Porter and Wentz's 1971 and 1972 models

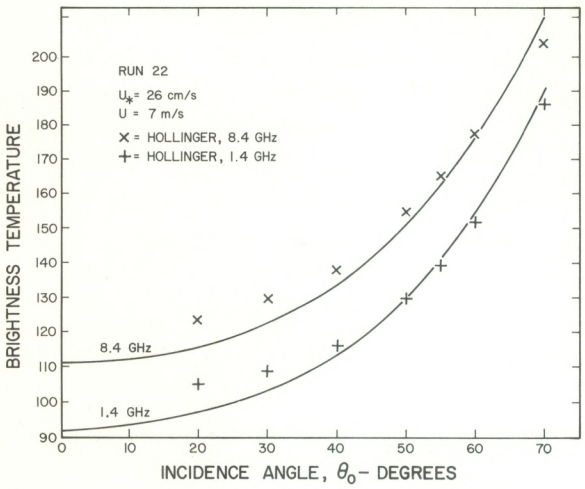

Figure 15.--Comparison of theoretical and measured brightness temperatures, 1.4 and 8.4 GHz. U is wind speed, and U_* is frictional velocity. Brightness temperatures are in kelvins.

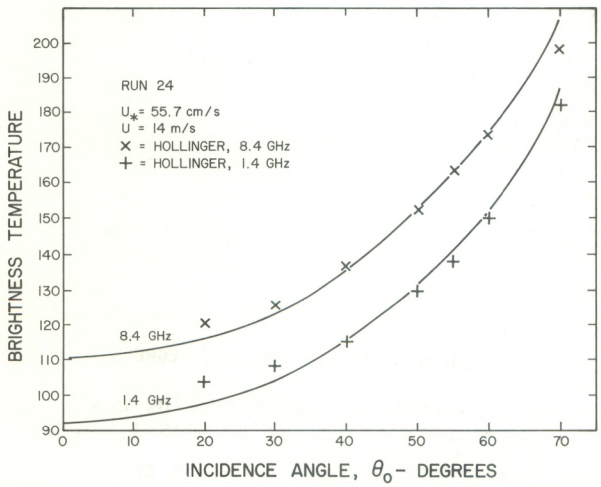

Figure 16.--Comparison of theoretical and measured brightness temperatures, 1.4 and 8.4 GHz. Brightness temperatures are in kelvins.

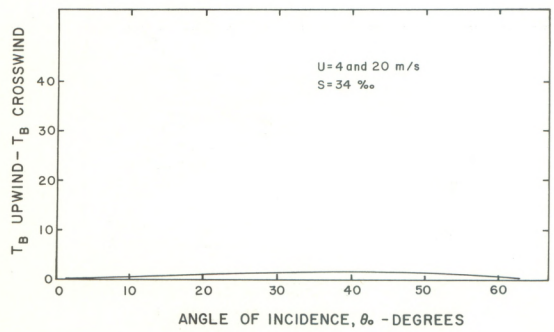

Figure 17.--Upwind-crosswind brightness temperature change, for unstable conditions f= 2.5 GHz, middle-latitude, and clear sky

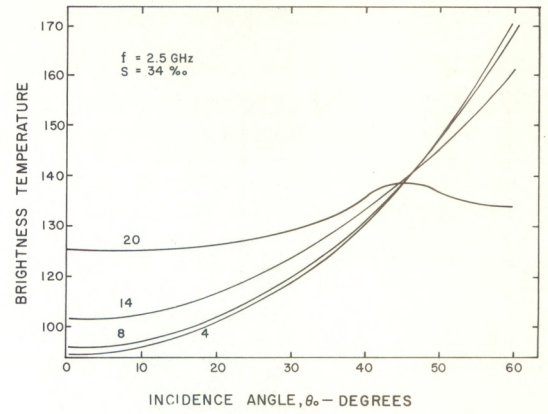

Figure 18.--Brightness temperature (kelvins) versus angle of incidence for wind speeds of 4, 8, 14, and 20 m/s. The conditions are middle-latitude, clear sky, and unstable.

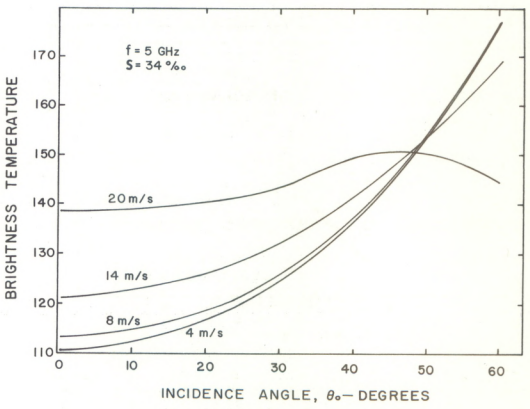

Figure 19.--Brightness temperature (kelvins) versus angle of incidence for wind speeds of 4, 8, 14, and 20 m/s. The conditions are middle-latitude, clear sky, and unstable.

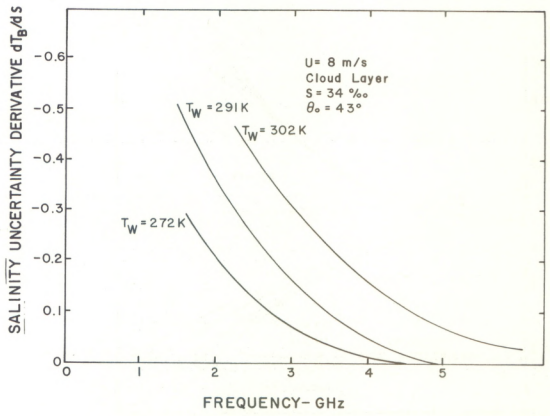

Figure 20.--Salinity uncertainty derivative versus frequency, U=8 m/s. Units of dT_B/dS are kelvins per part per thousand. T_W is water temperature.

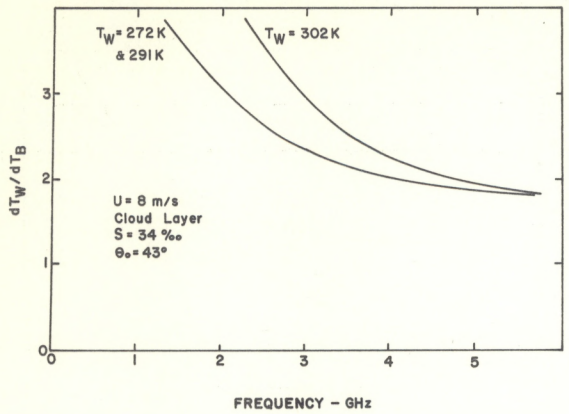

Figure 21.--Water temperature to brightness temperature derivative versus frequency

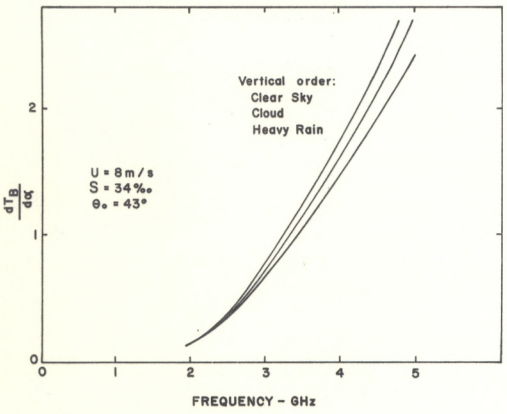

Figure 22.--Atmospheric uncertainty derivative versus frequency for middle-latitude conditions. The units of $dT_B/d\alpha$ are kelvins per millineper.

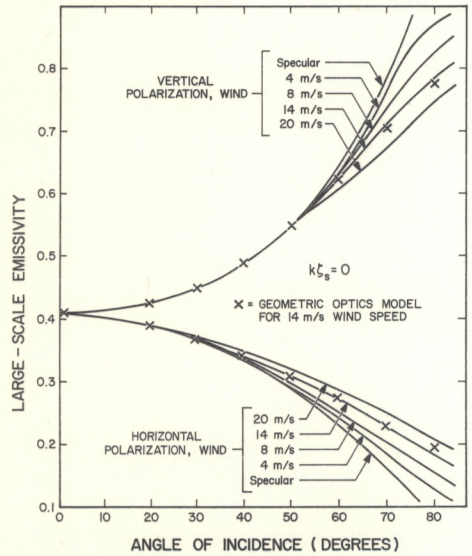

Figure 23.--Comparison of large-scale models for f=19.35 GHz

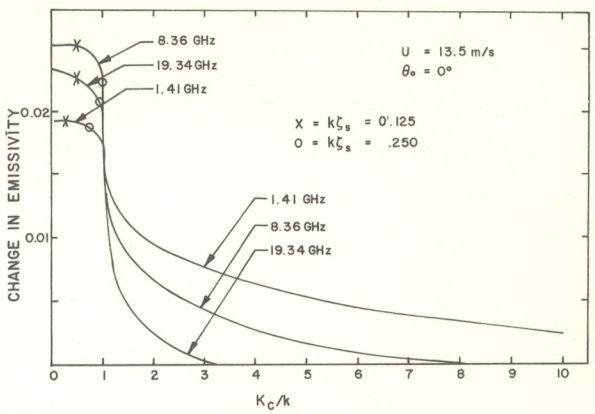

Figure 24.--Change in emissivity versus cutoff wave number

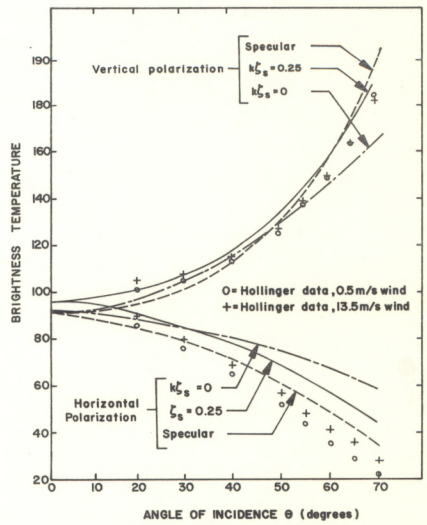

Figure 25.--Sea brightness temperatures versus incidence angle at 1.41 GHz

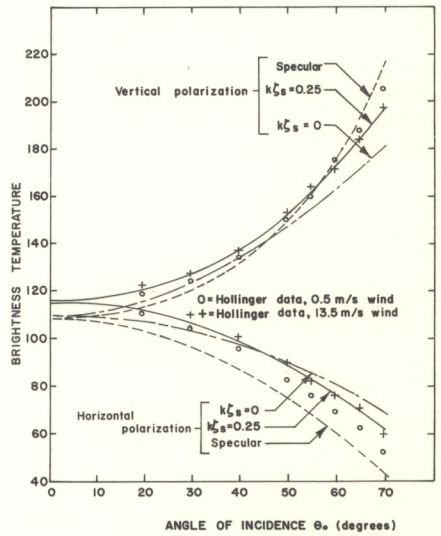

Figure 26.--Sea brightness temperatures versus incidence angle at 8.36 GHz

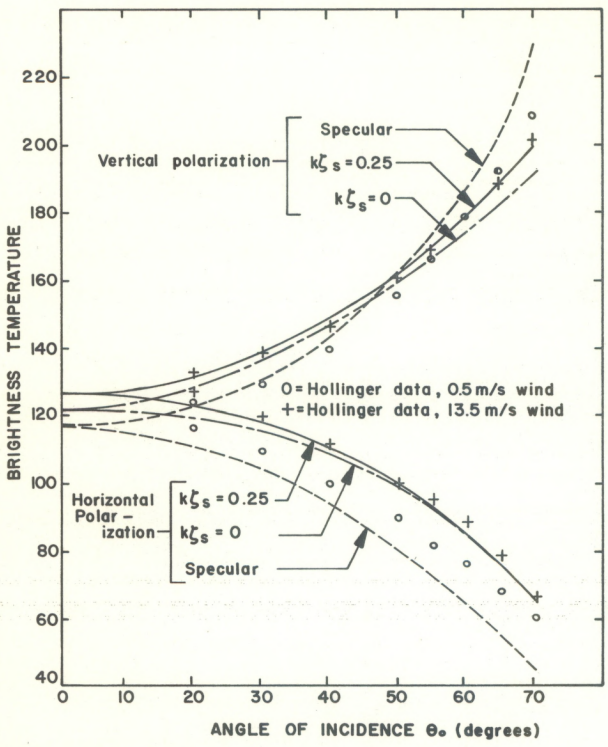

Figure 27.--Sea brightness temperatures versus incidence angle at 19.34 GHz

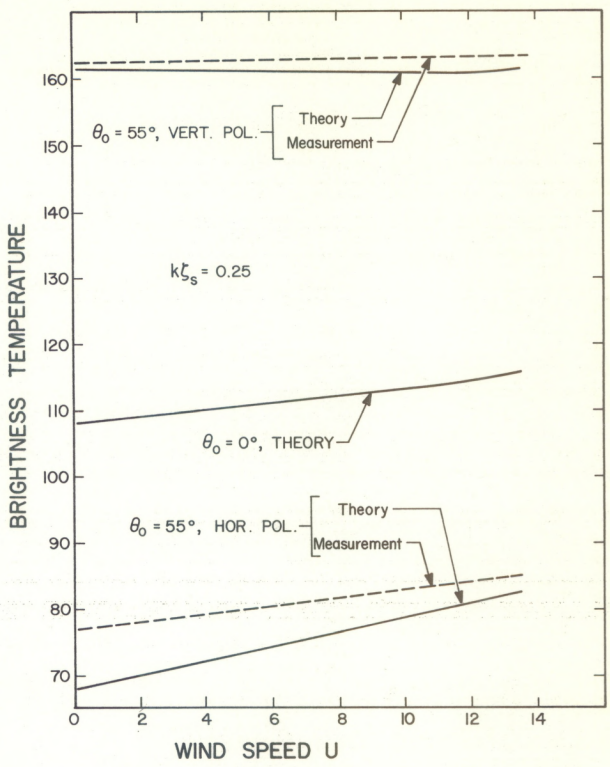

Figure 29.--Sea brightness temperatures versus wind speed (m/s) at 8.36 GHz

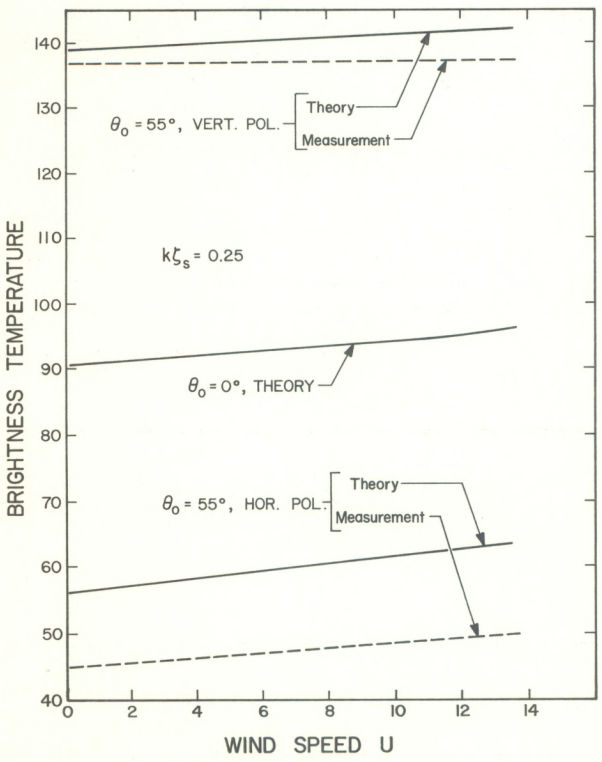

Figure 28.--Sea brightness temperatures versus wind speed (m/s) at 1.41 GHz

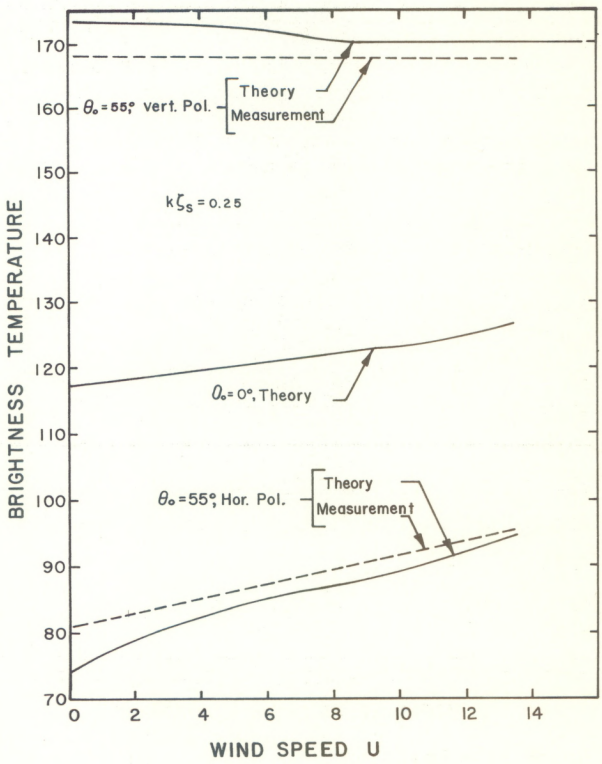

Figure 30.--Sea brightness temperatures versus wind speed (m/s) at 19.34 GHz

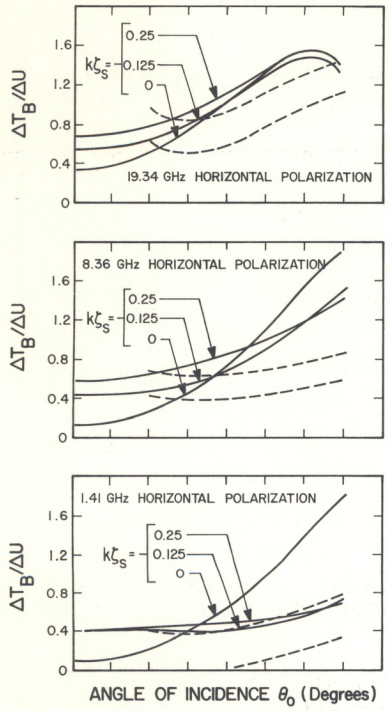

Figure 31.--Wind speed dependence of the horizontal component of brightness temperature. The dashed curves denote the range of Hollinger's data. The units of $\Delta T_B/\Delta U$ are kelvins per meter per second.

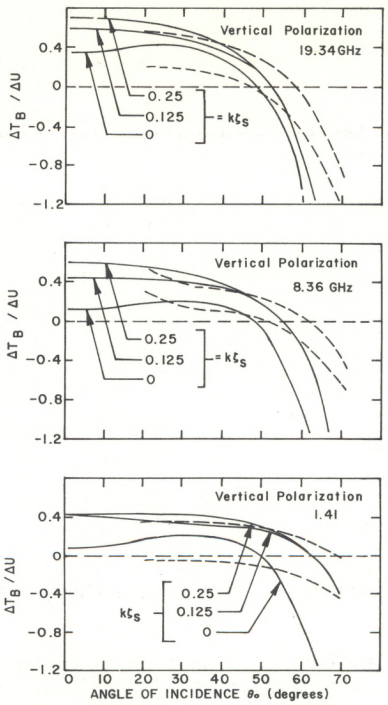

Figure 32.--Wind speed dependence of the vertical component of brightness temperature. The dashed curves denote the range of Hollinger's data. The units of $\Delta T_B/\Delta U$ are kelvins per meter per second.

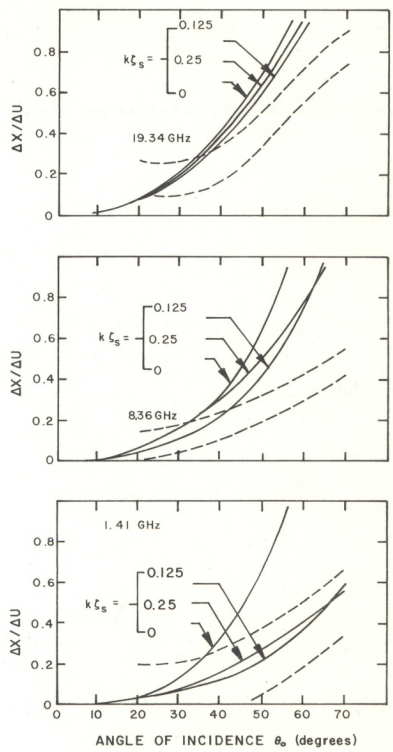

Figure 33.--Wind speed dependence of the percentage polarization, X. The dashed curves denote the range of Hollinger's data. The units of $\Delta X/\Delta U$ are percent per meter per second.

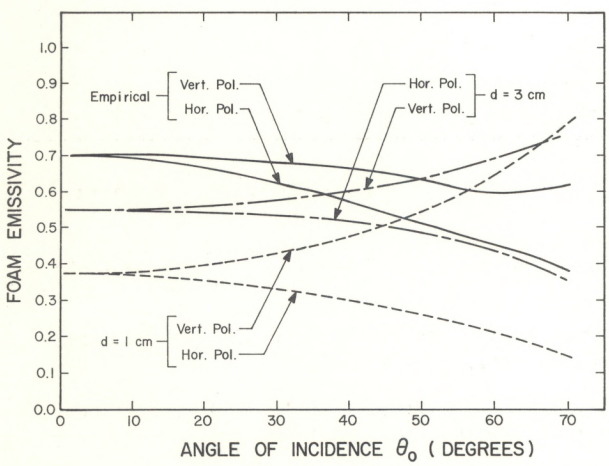

Figure 34.--Emissivity of a layer of foam of thickness d atop a flat sea surface, at 2.65 GHz

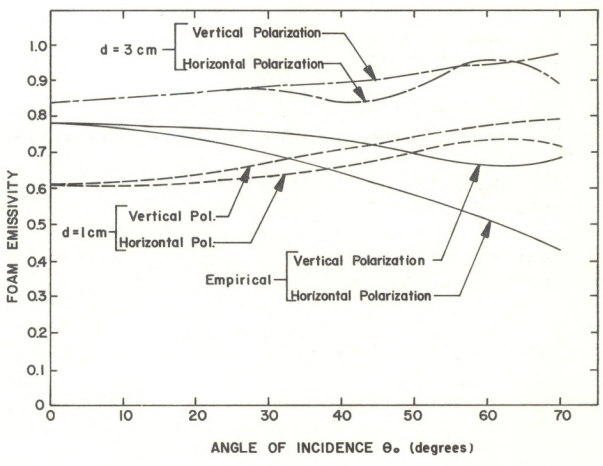

Figure 35.--Emissivity of a layer of foam of thickness d atop a flat sea surface, at 13.4 GHz

(Continued from inside front cover)

NESS 43 Cloud Motions in Baroclinic Zones. Linwood F. Whitney, Jr., October 1972, 6 pp. (COM-73-10029)

NESS 44 Estimation of Average Daily Rainfall From Satellite Cloud Photographs. Walton A. Follansbee, January 1973, 39 pp. (COM-73-10539)

NESS 45 A Technique for the Analysis and Forecasting of Tropical Cyclone Intensities From Satellite Pictures (Revision of NESS 36). Vernon F. Dvorak, February 1973, 19 pp. (COM-73-10675)

NESS 46 Publications and Final Reports on Contracts and Grants, 1972. NESS, April 1973, 10 pp. (COM-73-11035)

NESS 47 Stratospheric Photochemistry of Ozone and SST Pollution: An Introduction and Survey of Selected Developments Since 1965. Martin S. Longmire, March 1973, 29 pp. (COM-73-10786)

NESS 48 Review of Satellite Measurements of Albedo and Outgoing Long-Wave Radiation. Arnold Gruber, July 1973, 12 pp. (COM-73-11443)

NESS 49 Operational Processing of Solar Proton Monitor Data. Louis Rubin, Henry L. Phillips, and Stanley R. Brown, August 1973, 17 pp. (COM-73-11647/AS)

NESS 50 An Examination of Tropical Cloud Clusters Using Simultaneously Observed Brightness and High Resolution Infrared Data From Satellites. Arnold Gruber, September 1973, 22 pp. (COM-73-11941/4AS)

NESS 51 SKYLAB Earth Resources Experiment Package Experiments in Oceanography and Marine Science. A. L. Grabham and John W. Sherman, III, September 1973, 72 pp. (COM 74-11740/AS)

NESS 52 Operational Products From ITOS Scanning Radiometer Data. Edward F. Conlan, October 1973, 57 pp. (COM-74-10040)

NESS 53 Catalog of Operational Satellite Products. Eugene R. Hoppe and Abraham L. Ruiz (Editors), March 1974, 91 pp. (COM-74-11339/AS)

NESS 54 A Method of Converting the SMS/GOES WEFAX Frequency (1691 MHz) to the Existing APT/WEFAX Frequency (137 MHz). John J. Nagle, April 1974, 18 pp. (COM-74-11294/AS)

NESS 55 Publications and Final Reports on Contracts and Grants, 1973. NESS, April 1974, 8 pp. (COM-74-11108/AS)

NESS 56 What Are You Looking at When You Say This Area Is a Suspect Area for Severe Weather? Arthur H. Smith, Jr., February 1974, 15 pp. (COM-74-11333/AS)

NESS 57 Nimbus-5 Sounder Data Processing System, Part I: Measurement Characteristics and Data Reduction Procedures. W.L. Smith, H. M. Woolf, P. G. Abel, C. M. Hayden, M. Chalfant, and N. Grody, June 1974, 99 pp. (COM-74-11436/AS)

NESS 58 The Role of Satellites in Snow and Ice Measurements. Donald R. Wiesnet, August 1974, 12 pp. (COM-74-11747/AS)

NESS 59 Use of Geostationary-Satellite Cloud Vectors to Estimate Tropical Cyclone Intensity. Carl. O. Erickson, September 1974, 37 pp. (COM-74-11762/AS)

NESS 60 The Operation of the NOAA Polar Satellite System. Joseph J. Fortuna and Larry N. Hambrick, November 1974, 127 pp.

NESS 61 Potential Value of Earth Satellite Measurements to Oceanographic Research in the Southern Ocean. E. Paul McClain, January 1975, 18 pp.

NESS 62 A Comparison of Infrared Imagery and Video Pictures in the Estimation of Daily Rainfall From Satellite Data. Walton A. Follansbee and Vincent J. Oliver, January 1975, 14 pp.

NESS 63 Snow Depth and Snow Extent Using VHRR Data From the NOAA-2 Satellite. David F. McGinnis, Jr., John A. Pritchard, and Donald R. Wiesnet, February 1975, 10 pp.

NESS 64 Central Processing and Analysis of Geostationary Satellite Data. Charles F. Bristor (Editor), in press, 1975.

NESS 65 Geographical Relations Between a Satellite and a Point Viewed Perpendicular to the Satellite Velocity Vector (Side Scan). Irwin S. Ruff and Arnold Gruber, in press, 1975.